arXiv:1108.1543v2 [quant-ph] 15 Mar 2012

Quantum process tomography of single photon quantum channels with controllable decoherence

A Shaham and H S Eisenberg

Racah Institute of Physics, Hebrew University of Jerusalem, Jerusalem 91904, Israel

E-mail: assaf.shaham@mail.huji.ac.il

Abstract. We characterized unital quantum channels of single photon polarization qubits. The channels are composed of two birefringent crystals and wave-plates, where their decoherence properties are controlled. An experimental comparison between two different depolarizing configurations was performed using a quantum process tomography procedure. The results are with a high fidelity to the theoretical predictions.

PACS numbers: 03.65.Yz, 42.25.Ja, 42.50.Lc

Submitted to: *Phys. Scr.*

In recent years, within the growing interest in quantum communication, many schemes have used the polarization of a single photon to encode a two level quantum system - a qubit [1]. Interactions between such a photon and other surrounding systems may result in a decoherence process where noise is added to the quantum information that is stored in the photon polarization. The possibility to control and characterize the properties of this noise enables the study of its effects on various quantum protocols. In particular, it will be possible to test the performance of quantum error correction schemes and the efficiency of quantum key distribution protocols [2, 3]. The construction of a quantum channel that can induce different types of noises is important also for the study of a quantum-classical transition that a system may experience [4, 5].

Implementing a channel with controlled depolarization properties is a challenging task, since light interacts very weakly with its environment. Such a channel can be realized with the aid of birefringent crystals which entangle the polarization degree of freedom with the photon's temporal degrees of freedom [6] or with its spatial degrees of freedom [7, 8]. In this work, we studied a depolarizing channel which couples between polarization and time of light of short coherence times [9]. It is composed of two birefringent crystals and wave plates. The coupling depends on the relative angle between the symmetry axes of the crystals, the wave-plate orientations and the initial polarization of the input state. Depolarization occurs because photon detection is insensitive to the temporal degrees of freedom.

The polarization state of a single-photon qubit can be described either by a density matrix operator $\hat{\rho}$ or, equivalently, by a point in the Poincaré sphere. The Cartesian coordinates of this point are the Stokes parameters $\overline{S} = \{S_1, S_2, S_3\}$. Here we use the convention that S_1 represents the linear horizontal and vertical polarizations ($|h\rangle$,$|v\rangle$), S_2 represents the linear polarizations plus and minus 45° ($|p\rangle = (|h\rangle + |v\rangle)/\sqrt{2}$, $|m\rangle = (-|h\rangle + |v\rangle)/\sqrt{2}$), and S_3 represents the circular polarizations ($|r\rangle = (|h\rangle + i|v\rangle)/\sqrt{2}$ and $|l\rangle = (i|h\rangle + |v\rangle)/\sqrt{2}$). The length of the Stokes vector $D = \sqrt{S_1^2 + S_2^2 + S_3^2}$ represents the state's degree of polarization. For polarized states, $D = 1$, while for partially polarized states, $D < 1$. Characterization of the polarization state may be performed by several projection measurements with the Quantum State Tomography (QST) procedure [10].

Consider an arbitrary quantum state $\hat{\rho}$ that serves as an input state to a quantum channel. The final state $\hat{\rho}'$ is derived from the mapping $\hat{\rho}' = \mathcal{E}(\hat{\rho})$ where $\mathcal{E}$ is the operation of the channel. The mapping $\mathcal{E}$ can be uniquely described by the elements of the positive and Hermitian matrix χ:

$$\mathcal{E}(\hat{\rho}) = \sum_{m,n} \chi_{mn} \hat{E}_m \hat{\rho} \hat{E}_n^{\dagger}, \tag{1}$$

where $\hat{E}_m$ are basis elements that span the space of $\hat{\rho}$. The elements of the χ matrix can be experimentally determined by a Quantum Process Tomography (QPT) procedure [11]. A QPT procedure for a single-qubit process requires four QST measurements of different input states. We note that these four states should not lay on the same plane in the Poincaré sphere representation. Assuming the process has some special symmetries

may reduce the number of QST measurements that are required for the reconstruction of the χ matrix. A complete positive and trace preserving process is a unital process if $\mathcal{E}(\hat{I}) = \hat{I}$. A unitality assumption for a single qubit process may reduce the number of QST measurements that are needed for the process chracterization to 3.

The aim of this work is to study theoretically and experimentally the processes of two depolarizing channel schemes. The first channel (Scheme I, see figure 1) is composed of two equal birefringent crystals and two half-wave plates. The crystals are fixed perpendicularly with respect to each other, and the rotatable wave plates are placed before and after the first crystal. The second channel (Scheme II, see figure 1) is composed also of two equal perpendicularly fixed birefringent crystals, but here a quarter-wave plate is placed in between them. For both depolarizing schemes the symmetry axes of the crystals define the linear $|h\rangle$ and $|v\rangle$ polarizations, and the zero angle of the wave plates is determined with respect to the horizontal polarization. The coupling between polarization and temporal modes of such a channel can be described as follows: every crystal induces a temporal delay t between the horizontally and vertically components of an input polarized wave packet. This temporal walk-off t depends on the crystal length L, its refractive index difference Δn and the speed of light c such that $t = L\frac{\Delta n}{c}$. In order to achieve a complete separation (i.e. loss of coherence between horizontal and vertical wave packets), we require that $t > t_c$, where t_c is the coherence time of the initial wave packets. We see that if there is no polarization rotation between the two perpendicular crystals of our schemes (i.e. a wave plate that is placed in between them is set to a zero angle), the second crystal compensates for the time delay that was caused by the first one and no depolarization occurs. If there is a polarization rotation between the two crystals, two or three different temporal modes will be occupied after the second crystal. Tracing out these temporal degrees of freedom while measuring the polarization state will result in depolarization. It is easy to calculate the processes that these channels induce for any angle of the wave plates because in both schemes the polarization is coupled to a maximum of three discrete temporal modes (for details see [9]). We emphasize that the wave plates act on any of these modes separately; thus they do not couple between the different temporal modes. Theoretical calculations of the processes for both schemes have shown that the processes are unital regardless of the orientation of any wave plate in the channel configurations.

Our experimental setup is shown in figure 1: a Ti:Sapphire pulsed laser with a 76 MHz repetition rate was frequency doubled in order to generate pulses with a wavelength of 390 nm. These pulses were focused into and collinearly down-converted in a 1 mm thick type-I BBO crystal. The 780 nm down-converted signal was filtered by a dichroic mirror (DM) and collimated with a lens (L2). One photon of the pair was probabilistically split by a beam splitter (BS) and was sent to a detector. The second photon was directed to the depolarizing channel. For the two depolarizing schemes, the birefringent phase of the depolarizing crystals was tuned so that the entire depolarizing channel will not affect the state when the wave plate angles are set to zero. Characterizing the polarization state of the depolarized photons was performed by wave

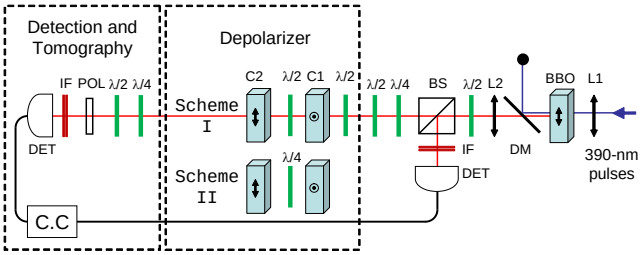

Figure 1: (Color online) The experimental setup and the depolarizing schemes. Laser pulses of 390 nm were focused by a lens (L1) into a BBO crystal and reflected by a dichroic mirror (DM). Down-converted signal was collimated by another lens (L2). One photon of the down-converted pair was probabilistically split by a beam splitter (BS) and detected by a single-photon detector (DET). The initial polarization state of the second photon was determined using half- and qurter-wave plates ($\lambda/2, \lambda/4$). The signal was directed to one of the two depolarizing schemes as shown. QST measurements were carried out using wave plates, a polarizer (POL) and another detector. The photons were temporally filtered using a 5 nm bandpass interference filters (IF). Spatial filtering was achieved with the coupling of the photons to single-mode fibres connected to the detectors.

plates and a polarizer (POL). Photons were filtered by 5 nm bandpass filters (IF), corresponding to a coherence time of $t_c \simeq 180$ fs, and then coupled into single-mode fibres, leading to single-photon detectors (DET). The detection of the second photon was conditioned by the detection of the first one in order to ensure that the depolarized signal is truly a quantum state.

The probabilistic nature of a quantum polarization state, together with systematic errors during the projection measurement procedure, may result in an illegal linear reconstruction of the measured state or the measured process. A Maximal Likelihood (ML) search that restricts the parameters to physically allowed values can be used to find the physical representation of $\hat{\rho}$ or χ that best fits to the tomographic data. We reconstructed all of the state density matrices using the ML protocol suggested by James *et al* [12]. As for the χ matrices, although ML searches for photonic QPT measurements were previously suggested and demonstrated [13, 14], we used a simpler ML search that gave sufficient results. According to the Choi-Jamiołkowski isomorphism, the linear mapping of a quantum channel represents a legal quantum state of a larger dimension [15]. Thus, we can assume that the linearly reconstructed process matrix χ_{linear} represents a four-dimensional (4D) quantum state. Additionally, we assume that this state was reconstructed from a set of 16 probability measurements $\{p_1, p_2, .., p_{16}\}$ obtained from 16 artificial projection measurements on the states $\{|\psi_1\rangle, ..., |\psi_{16}\rangle\}$. Inverting the linear reconstruction of a density matrix from the 16 probability measurements, we calculated these artificial probability values from χ_{linear}. Then, we reconstructed a new χ matrix using the artificial probability values with an ML quantum state search. We emphasis that χ might not be the process with the best fit to the data, but only a close physical fit to the originally measured data.

As this ML search requires the translation of the artificial probability measurements to a set of artificial counts, there is an extra free multiplying parameter $\mathcal{N}$. For example,

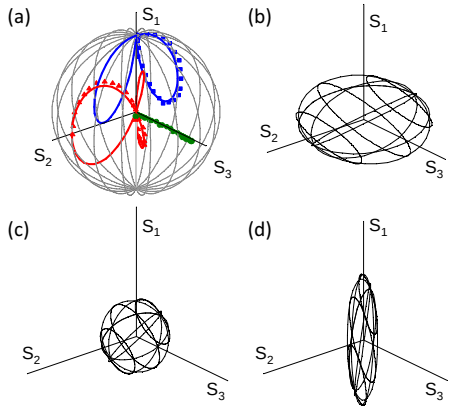

Figure 2: (Color online) The first depolarizing scheme: experimentally measured final states and QPT in the Poincaré sphere representation. (a) Comparison of final state measurements for input states of $|h\rangle$ (blue squares), $|p\rangle$ (red triangles), and $|r\rangle$ (green circles) in the range $0° < \theta < 90°$ and the theoretical model. Theoretical curves are presented as solid lines in the range $0° < \theta < 180°$. (b-d) Mapping of the surface of the Poincaré sphere to depolarized wire-mesh ellipsoids that were obtained by experimental QPT for the crystal angle values of (b) $\theta = 35.3°$, (c) $\theta = 54.74°$, and (d) $\theta = 67.5°$.

this parameter can represent the measurement time. We chose $\mathcal{N}$ such that the artificial set of counts will have the same order of magnitude as the actual qubit measured counts, which was about 25,000. Changing $\mathcal{N}$ had a minute effect on the χ matrix: multiplying or dividing $\mathcal{N}$ by 10^3 resulted in χ matrices whose fidelities with the original χ matrix $(F(\chi_1, \chi_2) = (\mathrm{Tr}\sqrt{\sqrt{\chi_1}\chi_2\sqrt{\chi_1}})^2)$ were higher than 99%. An error estimation of 2% for the process matrix fidelities and their eigenvalues resulted mainly from this fact.

Beginning with the first scheme, we rotated the two half-wave plates in opposite directions by an angle of $\theta/2$. This rotation is equivalent to the rotation of the first crystal by an angle of θ. We generated initial $|h\rangle$, $|p\rangle$ and $|r\rangle$ polarization states, sent them through the depolarizer and performed QST to the depolarized states for different θ angles in the range of $0 < \theta < 90°$. The traces of the measured states in the Poincaré sphere representation are shown in figure 2(a). Solid lines represent the theoretical calculations for angles in the range $0 < \theta < 180°$. Figures 2(b)-(d) present the measured process of the channel mapping of the Poincaré sphere surface when $\theta = 35.3° = \tan^{-1}(\frac{1}{\sqrt{2}})$, $\theta = 54.7° = \tan^{-1}(\sqrt{2})$, and $\theta = 67.5°$, respectively. The initial states that were used for the QPT were $|h\rangle$, $|p\rangle$ and $|r\rangle$, where the process of $\theta = 35.3°$ was reconstruct using the unitality assumption, and the other two processes were measured using the additional input state of $|v\rangle$. The first process (figure 2 (b)) maps the surface of the Poincaré sphere to an ellipsoid with two primary radii of length $\frac{2}{3}$ and the third one has a length of $\frac{1}{3}$. The second process (figure 2 (c)) is an isotropic depolarizing process that maps the polarized states to a sphere with radius equal to $\frac{1}{3}$. The third process (figure 2 (d)) corresponds to a mapping of the Poincaré sphere surface to an ellipsoid with one primary radius with a length of ~ 0.7 and two primary radii with a length of ~ 0.15.

In order to evaluate the channel performance with respect to the theoretical

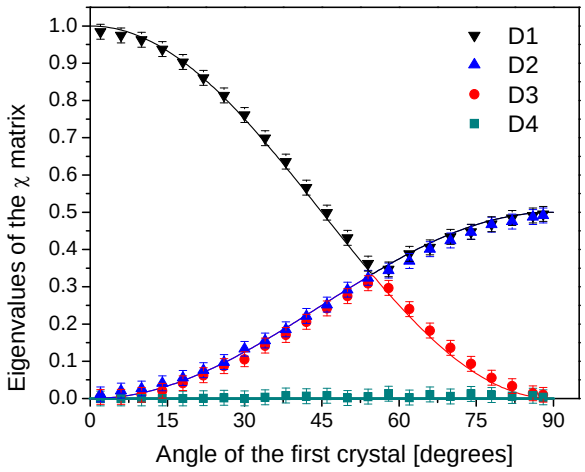

Figure 3: (Color online) The eigenvalues of the χ matrix as a function of the equivalent first-crystal rotation angle θ for the first depolarizing scheme.

prediction, we compared between the measured χ matrices and the theoretically calculated χ_d matrices. A comparison between the three measured maps that are presented in figure 2(b)-(d) and the theoretically calculated maps resulted with fidelities F higher than $97 \pm 2\%$.

A systematic study of the decoherence that the first scheme can induce can be performed by exploring the eigenvalues of the 4D χ matrix as a function of the angle θ. Since they are not affected by rotations and reflections of the input state, these eigenvalues may serve as a measure of the pure decoherence types that a quantum state may experience while passing through the channel. Using the assumption of unitality, we have used the transformed states that are presented in figure 2(a) to reconstruct the χ matrix for the range of angles $0 < \theta < 90°$. The measured eigenvalues of these matrices are presented in figure 3 along with their theoretical predictions. We see that only three eigenvalues participate in the process, while the fourth eigenvalue remains zero for every angle. Two eigenvalues out of these three are always equal. When the process is isotropic ($\theta = 54.7°$) the three eigenvalues intersect and are equal to $\frac{1}{3}$.

Moving to the second depolarizing scheme, we characterized the channel process for different angles ϕ of the quarter-wave plate in the range of $0 < \phi < 90°$. The QPT was performed by three QST measurements for outputs of the three initial mutually unbiased states $\overline{S}_a = \{\sqrt{1/3}, 0, -\sqrt{2/3}\}$, $\overline{S}_b = \{\sqrt{1/3}, \sqrt{1/2}, \sqrt{1/6}\}$, and $\overline{S}_c = \{\sqrt{1/3}, -\sqrt{1/2}, \sqrt{1/6}\}$. It is worth mentioning that these three states have the property that their final output state after passing through the second scheme has the same degree of polarization regardless of the angle ϕ. Using the assumption of unitality, we reconstruct the χ matrices of the different processes. The eigenvalues of these matrices and their theoretical predictions are presented in figure 4. As in the first scheme, only three eigenvalues participate in the process, and two out of them are equal for any orientation of the quarter-wave plate. Maximal decoherence is obtained when

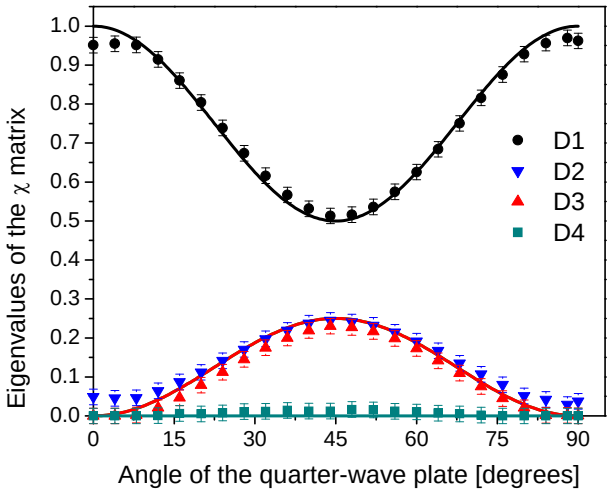

Figure 4: (Color online) The eigenvalues of the χ matrix as a function of the quarter-wave plate angle ϕ for the second depolarizing scheme.

$\phi = 45°$, where the eigenvalues are $\frac{1}{2}$, $\frac{1}{4}$, $\frac{1}{4}$ and 0. As can be seen in figure 3, the same eigenvalues of the χ matrix are obtained also with the first scheme when $\theta = 45°$. A comparison between the measurements of these two processes is shown in figure 5: the mapping of the surface of the Poincaré sphere according to scheme I process at $\theta = 45°$ and the real and the imaginary parts of the χ matrix are shown in figure 5(a)-(c), respectively. The mapping and the real and imaginary part of the χ matrix that are shown in figure 5(d)-(f) correspond to the scheme II process at $\phi = 45°$. Both processes map the Poincaré sphere into the shape of a disk, but the rotations that accompany the processes are different. This is reflected in the difference between the elements of the χ matrices and in the difference in the orientation of the wire mesh of the mapping. The fidelities of these two measured processes to the desired ones are $97 \pm 2\%$ and $98 \pm 2\%$ for the first scheme process at $\theta = 45°$, and the second scheme process at $\phi = 45°$, respectively.

In conclusion, we characterized the processes of two depolarizing schemes composed of two perpendicularly fixed equal birefringent crystals, and rotatable wave plates. All processes were analyzed according to the eigenvalues of their χ matrix which serve as a measure for the decoherence properties. The schemes realize processes in which three eigenvalues of the χ matrix differ from zero, and two out of them are equal. A comparison of scheme I which contains a half-wave plate in between the crystals and scheme II which contains a quarter-wave plate in between them reveals that scheme I offers more possible decoherence types than Scheme II. Both schemes exhibit high fidelities to the theoretical predictions. Ongoing research on the decoherence of more composite quantum systems is currently in progress using these depolarizing schemes.

The authors thank Jan Soubusta and Karel Lemr for a helpful discussion, and the Israeli Science Foundation for supporting this work under Grant No. 366/06.

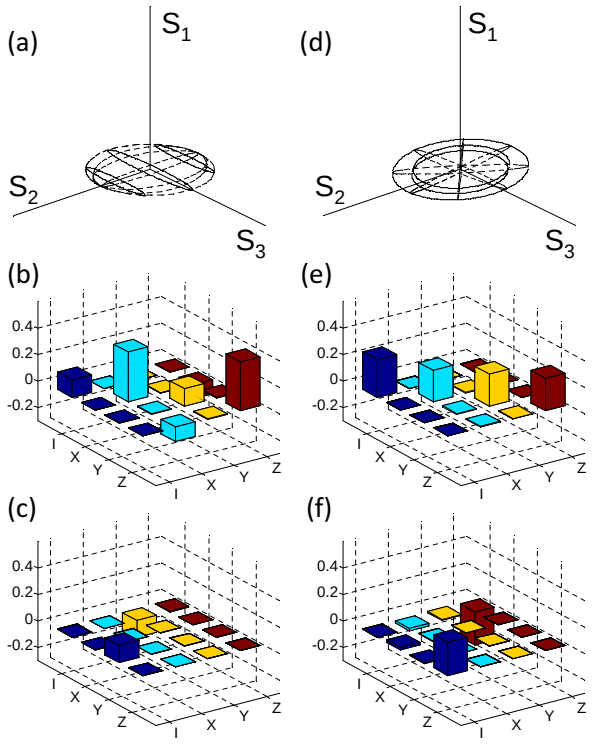

Figure 5: (Color online) A comparison between the disk mapping processes of the first scheme and the second scheme. (a-c) Measured mapping of the surface of the Poincaré sphere, real and imaginary parts of the χ matrix for the first scheme process of $\theta = 45°$. (d-f) The corresponding results for the $\phi = 45°$ second scheme process.

References

[1] Nielsen M A and Chuang I L 2000 *Quantum Computation and Quantum Information* (Cambridge: Cambridge University Press)

[2] Bennett C H and Brassard G 1984 *Proceedings of the IEEE International Conference on Computers, Systems and Signal Processing (Bangalore, India)* (IEEE, New York) 175-79

[3] Bruß D 1998 *Phys. Rev. Lett.* **81** 3018

[4] Almeida M P, de Melo F, Hor-Meyll M, Salles A, Walborn S P, Ribeiro P H S and Davidovich L 2007 *Science* **316** 579-82

[5] Xu J S, Li C F, Gong M, Zou X B, Shi C H, Chen G and Guo G C 2010 *Phys. Rev. Lett.* **104** 100502

[6] Kwiat P G, Berglund A J, Altepeter J B and White A G 2000 *Science* **290** 498-501

[7] Nambu Y, Usami K, Tomita A, Ishizaka S, Hiroshima T, Tsuda Y, Matsumoto K and Nakamura K 2002 *Proc. SPIE Int. Soc. Opt. Eng* Vol 4917 p 13

[8] Puentes G, Voigt D, Aiello A and Woerdman J P 2006 *Opt. Lett.* **31** 2057-59

[9] Shaham A and Eisenberg H S 2011 *Phys. Rev. A* **83** 022303

[10] Altepeter J B, Jeffrey E R and Kwiat P G 2005 *Adv. At. Mol. Opt. Phys.* **52** 105-59

[11] Chuang I L and Nielsen M A 1997 *J. Mod. Opt.* **44** 2455-67

[12] James D F V, Kwiat P G, Munro W J, and White A G 2001 *Phys. Rev. A* **64** 052312

[13] OBrien J L, Pryde G J, Gilchrist A, James D F V, Langford N K, Ralph T C and White A G 2004 *Phys. Rev. Lett.* **93** 080502

[14] Jezek M, Fiurasek J and Hradil Z 2003 *Phys. Rev. A* **68** 012305

[15] Jamiołkowski A 1972 *Rep. Math. Phys.* **3** 275-78